Chemistry & Biology
Article

The Binding Avidity of a Nanoparticle-Based Multivalent Targeted Drug Delivery Platform

Seungpyo Hong,[1,5] Pascale R. Leroueil,[4,5] István J. Majoros,[5] Bradford G. Orr,[3,5] James R. Baker, Jr.,[5,*] and Mark M. Banaszak Holl[1,2,4,5,*]
[1] Program in Macromolecular Science and Engineering
[2] Program in Biophysics
[3] Department of Physics
[4] Department of Chemistry
[5] Michigan Nanotechnology Institute for Medicine and Biological Sciences
University of Michigan, Ann Arbor, MI 48109, USA
*Correspondence: jbakerjr@umich.edu (J.R.B.), mbanasza@umich.edu (M.M.B.H.)
DOI 10.1016/j.chembiol.2006.11.015

SUMMARY

Dendrimer-based anticancer nanotherapeutics containing ~5 folate molecules have shown in vitro and in vivo efficacy in cancer cell targeting. Multivalent interactions have been inferred from observed targeting efficacy, but have not been experimentally proven. This study provides quantitative and systematic evidence for multivalent interactions between these nanodevices and folate-binding protein (FBP). A series of the nanodevices were synthesized by conjugation with different amounts of folate. Dissociation constants (K_D) between the nanodevices and FBP measured by SPR are dramatically enhanced through multivalency (~2,500- to 170,000-fold). Qualitative evidence is also provided for a multivalent targeting effect to KB cells using flow cytometry. These data support the hypothesis that multivalent enhancement of K_D, not an enhanced rate of endocytosis, is the key factor resulting in the improved biological targeting by these drug delivery platforms.

INTRODUCTION

Multivalent interactions, the simultaneous binding event of multiple ligands to multiple receptors in biological systems, have been extensively investigated to promote targeting of specific cell types [1–7]. These activities are also central to a number of pathological processes, including the attachment of viral, parasitic, mycoplasmal, and bacterial pathogens [8–13]. The design of synthetic systems has been approached primarily through the development of multivalent inhibitors. Studies with biological multivalent inhibitors have yielded quantitative measurements of binding avidities, with increases on the order of 1 to 9 orders of magnitude [14–18]. In contrast, synthetic multivalent effectors have exhibited much smaller improvements in binding avidities, ranging from just 1 to 2 orders of magnitude. Design and implementation of effective synthetic multivalent effector platforms capable of effectively targeting desired cell types in vivo remain important challenges.

Selective targeting of therapeutics to cancer cells is desirable to improve treatment outcomes and to avoid toxic side effects. The vitamin folic acid (FA), which has a high affinity for the folate receptor (FAR), has been employed as a specific targeting moiety [1] since FAR is overexpressed in many epithelial cancer cells, including breast, ovary, endometrium, kidney, lung, head and neck, brain, and myeloid cancers [19–22]. A variety of FA conjugates and complexes have been developed for tumor-specific targeting [2]. These include protein toxins [23], low molecular weight chemotherapeutics [24], immunotherapeutic agents [25], drug entrapped liposomes [26], and organic/inorganic nanoparticles [3–5]. However, the affinities of these folate targeting systems are limited by the number of FA molecules attached to the drugs and/or by the topology of their chemical structures. This has, in some cases, resulted in insufficient drug delivery efficiency to target cancer cells [27]. The best directly measured results to date employing multivalent FA conjugates showed ~10- to 100-fold enhancement over free FA [5].

Recently, a series of papers has been published describing the design, synthesis, in vitro cell experiments, and mouse xenograft (KB cells) testing of a drug delivery device based upon a generation 5 poly(amidoamine) (G5 PAMAM) scaffold, to which ~5 folic acid molecules, dye, and methotrexate had been conjugated [6, 28–30]. The in vivo improvement in efficacy of this nanodevice over free drug was attributed to a multivalent interaction between the multiple FA groups on the dendrimer periphery with multiple high-affinity receptors on the tumor cell surfaces. In order to test this hypothesis, a series of acetamide-terminated G5 dendrimer scaffolds containing ~2–14 folic acid molecules and AlexaFluor 488 dye (AF488) were synthesized (G5-Ac-AF488-FA_x). Quantitative measurements of K_D were obtained for the interaction of the devices with surface immobilized folate binding protein (FBP) by using surface plasmon resonance (SPR). Remarkably, these effector systems exhibit a ~2,500- to

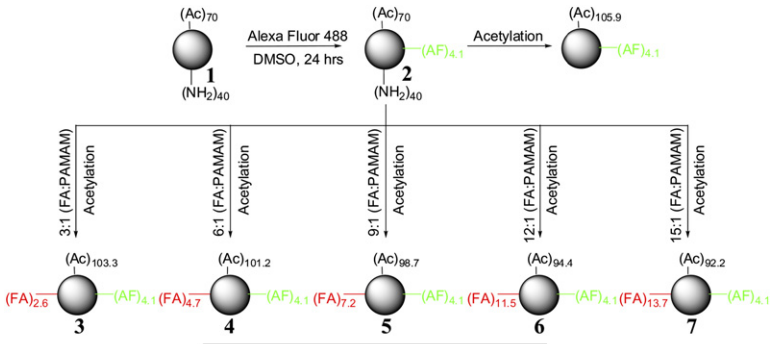

Nanodevice	M_n	PDI
1	29,470	1.03
2	31,660	1.11
3	32,820	1.17
4	33,750	1.30
5	34,840	1.72
6	36,730	4.67
7	37,700	12.41

Figure 1. Synthetic Scheme for G5 PAMAM Dendrimer-Based Nanodevices with AF488 and Different Numbers of FA Molecules

The number average molecular weights and PDIs were determined by GPC. All numbers of functional attachment were calculated from GPC results. The total number of end groups (110) was determined by potentiometric titration [40].

~170,000-fold enhancement of binding avidities as compared to free FA. Qualitative studies of G5-Ac-AF488-FA_x to KB cells performed at 37 and 4°C and analyzed using a fluorescence activated cell sorter (FACS) showed the same general trend in surface binding regardless of temperature (low temperature prevents internalization but not binding). The significance of this data is 3-fold: (1) the ability of PAMAM dendrimer-based scaffolds to afford a functional multivalent effector system is demonstrated; (2) the in vivo effect is demonstrated to arise from the substantial enhancement of K_D, not an increased rate of endocytosis; and (3) the on-rate, k_a, increases linearly with the number of targeting agents and shows no cooperativity, whereas the off-rate, k_d, decreases exponentially with the number of targeting agents.

RESULTS

Synthesis and Characterization of G5 PAMAM Dendrimer-Based Nanodevices

The PAMAM dendrimer-based FAR targeting nanodevices were synthesized as summarized in Figure 1. AF488 was first attached to the partially acetylated G5 PAMAM dendrimers, with a range of different numbers of FA then attached to the dendrimer/AF488 conjugates, yielding the dendritic nanodevice products. Since all the nanodevices were conjugated with the same number of AF488, differences in fluorescence intensities from the nanodevices in later FACS data can be regarded as a result of differences in nanodevice binding and/or uptake by KB cells. As the last step of the synthesis, remaining terminal amine groups were fully acetylated to prevent nonspecific electrostatic interactions [31, 32]. This last step is particularly important because remaining amine termini in the dendrimers protonate at physiological pH and cause nonspecific binding and uptake in vitro and in vivo as well as nonspecific binding with the carboxylate-terminated dextran surface of the SPR sensor chips. Full acetylation is thus necessary to accurately quantify the receptor-specific interactions in both SPR and FACS studies. These dendrimer nanodevices were characterized spectroscopically using ^{1}H NMR and UV/Vis as well as chromatographically using GPC and HPLC (Table 1 and Figure 1; see Figures S1, S2, S3, and S4 in the Supplemental Data available with this article online). The nanodevices become more polydisperse and ultimately give a bimodal distribution as the number of attached FA increases. In the case of G5-Ac-AF488-$FA_{13.7}$, the polydispersity index (PDI) is 12.41 which is significantly greater than PDIs of previously reported dendrimer conjugates. In accordance with this finding, the full width at half-maximum of the HPLC peaks also broadened as expected (see Figure S3) [33].

The mean number of FA per dendrimer was calculated from GPC data as shown in Table 1. UV/Vis measurements were consistent with an increasing amount of FA per dendrimer but were systematically lower than the GPC values. The FA is confined to the dendrimer surface, creating an effectively higher local concentration, and thus shows an expected deviation from Beer's Law.

Quantitative Binding Avidities between the Nanodevices and Surface-Bound FBP Measured Using Surface Plasmon Resonance

Dissociation constants (K_D) for the binding of G5-Ac-AF488-FA_x nanodevices with surface-bound FBP are listed in Table 2 (for the SPR sensorgram traces, see Figure S7). K_D of free FA was measured to be ~5 × 10^{-6} M, in good agreement with a previously reported value (~11 × 10^{-6} M) obtained by SPR [5]. Our negative control (G5-Ac-AF488) without targeting moiety FA shows no specific or nonspecific binding, indicating the nontargeted nanodevices do not significantly interact with the carboxylated dextran surface of the sensor chip or the FBP immobilized channel. When employing G5-Ac-AF488-$FA_{2.6}$, a significant degree of binding in the channel with immobilized FBP was observed, whereas no detectable binding took

Table 1. Calculation of Numbers of FA Attached on a Dendrimer Molecule Determined by GPC and UV

Nanodevices[a]	Nominal Equiv. #FA Added for FA Conjugation	#FA (GPC)[b]	#FA (UV)[c]
G5-Ac-AF488-FA_0	0	—	—
G5-Ac-AF488-$FA_{2.6}$	3	2.6	1.3 ± 0.3
G5-Ac-AF488-$FA_{4.7}$	6	4.7	3.0 ± 0.2
G5-Ac-AF488-$FA_{7.2}$	9	7.2	5.3 ± 0.2
G5-Ac-AF488-$FA_{11.5}$	12	11.5	8.3 ± 0.9
G5-Ac-AF488-$FA_{13.7}$	15	13.7	10.6 ± 1.8

[a] The subscripted numbers of FA are the values determined by GPC in the third column.
[b] The numbers were calculated by dividing the molecular weight difference by the molecular weight of free FA.
[c] The numbers were determined by UV from two sets of data. The calculation was performed by comparing UV absorbance of the nanodevices with a standard curve made by the absorbance of free FA at different concentrations. The values were averaged from the two sets of data and are presented with standard deviations.

place in the reference channel (carboxylated dextran surface). The measured K_D is $\sim 2 \times 10^{-9}$ M, which is a ~2500-fold increase in avidity per dendrimer particle or a ~1000-fold increase in binding avidity as a function of total FA concentration. The G5-Ac-AF488-$FA_{4.7}$ device exhibited per particle binding avidity improvements of two orders of magnitude enhancement in the K_D value ($\sim 7 \times 10^{-11}$ M) as compared to the G5-Ac-AF488-$FA_{2.6}$ and five orders of magnitude improvement as compared to free FA. Further increasing the number of FAs (7.2, 11.5, and 13.7) conjugated to the nanodevices did not produce similar increases in the magnitude of binding avidities. Instead, more modest gains related to the simple increase in total FA concentration were achieved (Figure 2). Nonetheless, the lowest K_D observed (G5-Ac-AF488-$FA_{13.7}$) is ~170,000 times lower than the K_D of free FA.

Table 2. Quantified Binding Constants of the Dendritic Nanodevices with FBP Measured by SPR

Targeted Nanodevice	Dissociation Constant K_D (M)[a]	Fold Increase over Free FA[b]	Fold Increase over Free FA[c]
Free FA	$5 \pm 3 \times 10^{-6}$	—	—
G5-Ac-AF488-$FA_{2.6}$	$2 \pm 1 \times 10^{-9}$	2,500	1,000
G5-Ac-AF488-$FA_{4.7}$	$7 \pm 6 \times 10^{-11}$	71,400	15,200
G5-Ac-AF488-$FA_{7.2}$	$7 \pm 2 \times 10^{-11}$	71,400	9,900
G5-Ac-AF488-$FA_{11.5}$	$5 \pm 1 \times 10^{-11}$	100,000	8,700
G5-Ac-AF488-$FA_{13.7}$	$3 \pm 2 \times 10^{-11}$	166,700	12,200

[a] Obtained by averaging at least three different runs of SPR measurements. The values are averages ± standard deviations taken from different runs.
[b] Fold increase based on dendrimer concentrations. Also known as multivalency parameter β.
[c] Fold increase based on FA concentrations.

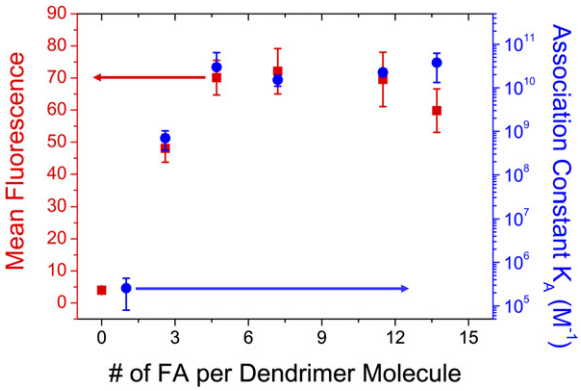

Figure 2. Comparison of the Model Study Using SPR and the In Vitro Study Using FACS of the Effect of the Number of FA per Dendrimer Molecule upon Binding Constant

Note that blue circles and red squares represent SPR and FACS results, respectively. The error bars represent standard deviations. The nanodevice with 2.6 FA shows a lower degree of cellular binding and association constant K_A than the rest of the nanodevices. FACS data were obtained after incubation with dendritic nanodevices with FAR-overexpressing KB cells at 37°C and represent averaging from 12 different samples at each condition. Association constants were averaged values from at least three SPR measurements for each point. The association constant ($K_A = 1/K_D$) is plotted in this case as it provides the best visual comparison to the FACS data.

Binding of the Nanodevices with FAR-Overexpressing KB Cells: FACS and CLSM

A confocal image of KB cells incubated with G5-Ac-AF488-$FA_{4.7}$ indicates that the nanodevices bind to the cell surface but do not substantially internalize into the KB cells after 1 hr incubation at 37°C (Figure 3). Concentration-dependent cellular binding of the G5-Ac-AF488-FA_x nanodevices to FAR-overexpressing KB cells was assessed by FACS. As shown in Figure 4A, G5-Ac-AF488-$FA_{2.6}$ exhibits a lower degree of binding after incubation with KB cells at 37°C for 1 hr than the rest of the nanodevices. This trend is consistent with the differences in K_D measured by SPR. Additional binding experiments were carried out at 4°C to explore the possible role of FAR membrane mobility on the measured binding constant. The identical behavior observed for cells at 37°C and 4°C suggests that the dendrimer conjugates interact with FAR that are preorganized on the cell membrane surface and that they do not assemble to form a preferred geometry in response to the G5-Ac-AF488-FA_x nanodevices.

To further compare the SPR results and the in vitro FACS results, a plot of cellular binding (FACS) and association constant K_A (SPR) against the number of FA per dendrimer molecule is shown in Figure 2. The K_A and mean fluorescence both initially increase significantly as a function of number of FAs attached to the dendrimer.

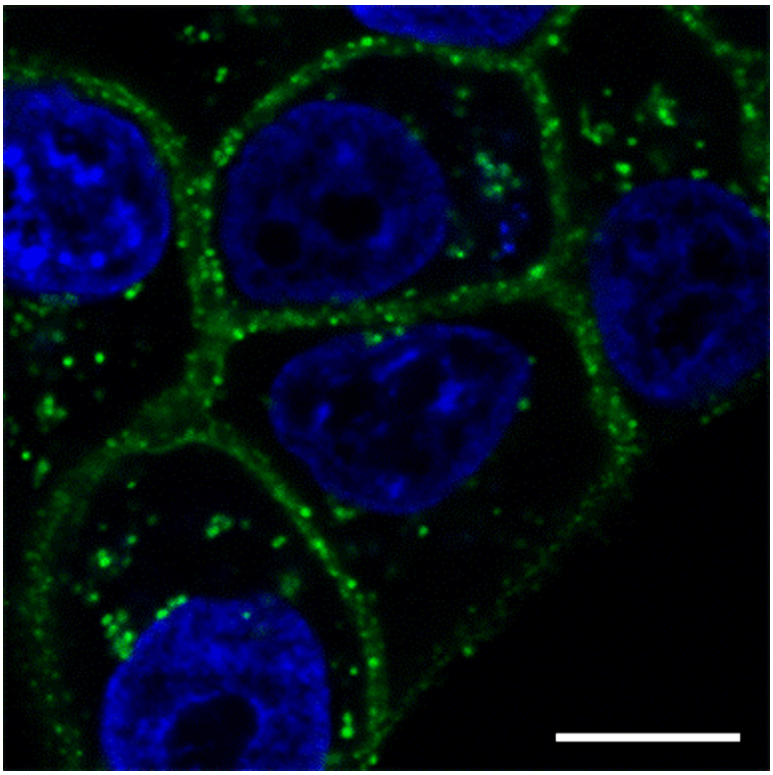

Figure 3. CLSM of Dendrimers, G5-Ac-AF488-$FA_{4.7}$, after Incubation with KB Cells at 37°C for 1 hr

Green fluorescence comes from AlexaFluor 488 (AF488) attached to the dendritic nanodevices, and blue fluorescence is cell nuclei stained by DAPI. Note that after 1 hr the dendrimers have bound to the cell surface but have not substantially internalized. This has been confirmed by independent Z stack confocal fluorescence microscopy images. Scale bar: 10 μm.

However, beginning with 7.2 FA per dendrimer, a plateau is also observed for cellular binding.

Quantitative Measurement of the On-Rate and Off-Rate Constants between the Nanodevices and Surface-Bound FBP Measured Using Surface Plasmon Resonance

In addition to quantitative measurement of K_D or K_A, which can be conveniently compared to the cell binding data determined by FACS, the SPR sensorgrams can also be analyzed to quantitatively determine the on-rates (k_a) and off-rates (k_d) for the nanodevices with the immobilized FBP. The on-rates were observed to increase linearly with the number of folic acids present on dendrimer. The off-rates were observed to decrease exponentially with an increase in the number of folic acids present. The dependence of both rate constants on the number of folic acids per dendrimer is illustrated in Figure 5.

DISCUSSION

Designed multivalent targeting systems offer great promise for enhancing the therapeutic index of a wide range of drugs [2, 4, 6, 24, 26, 36]. Particularly, multivalently targeting devices can provide dramatic improvements in avidity by enhancing the resident time of the drug on the cell target [29]. The ~2,500- to 170,000-fold improvements in binding avidity as measured by K_D are, to the best of our knowledge, the most potent demonstration to date of a multivalent effector system. As already noted, this dramatic improvement in K_D has already been shown to translate into an ability to selectively target and kill FAR-bearing cancer cells both in vitro and in vivo [6, 29, 37, 38].

The cooperativity of a multivalent system can be defined as shown in Equation (1), where K is the dissociation constant, N is the number of ligands, and α is the degree of cooperativity.

$$K_N^{multi} = (K^{mono})^{\alpha N} \quad (1)$$

Multivalent interactions are defined as positively cooperative for $\alpha > 1$, noncooperative for $\alpha = 1$, and negatively cooperative for $\alpha < 1$. The data presented in this paper show $K^{mono} = 5 \times 10^{-6}$, $K_{2.6} = 2 \times 10^{-9}$, and $K_{4.7} = 7 \times 10^{-11}$, which is $K_{2.6} < (K^{mono})^{2.6}$ and $K_{4.7} < (K^{mono})^{4.7}$ (Table 2). Thus, G5-Ac-AF488-FA_x is a negatively cooperative multivalent system as anticipated based upon the results obtained from all other experimental multivalent systems to date [10]. The data can also be considered using the alternative multivalency parameter β as indicated in Equation 2 [10].

$$K_N^{multi} = \beta K^{mono} \quad (2)$$

Our empirical measurements exhibit $\beta(K_{2.6})$ = 2,500, $\beta(K_{4.7})$ = 71,000, $\beta(K_{7.2})$ = 71,000, $\beta(K_{11.5})$ = 100,000, and $\beta(K_{13.7})$ = 170,000 as shown in Table 2, consistent with a multivalent interaction.

The SPR data can be further analyzed in terms of the on-rate (k_a) and the off-rate (k_d) of the dendrimer with the FBP surface (Figure 5). The linear increase in k_a as a function of number of folic acid ligands indicates that the association to the surface does not exhibit any cooperativity or

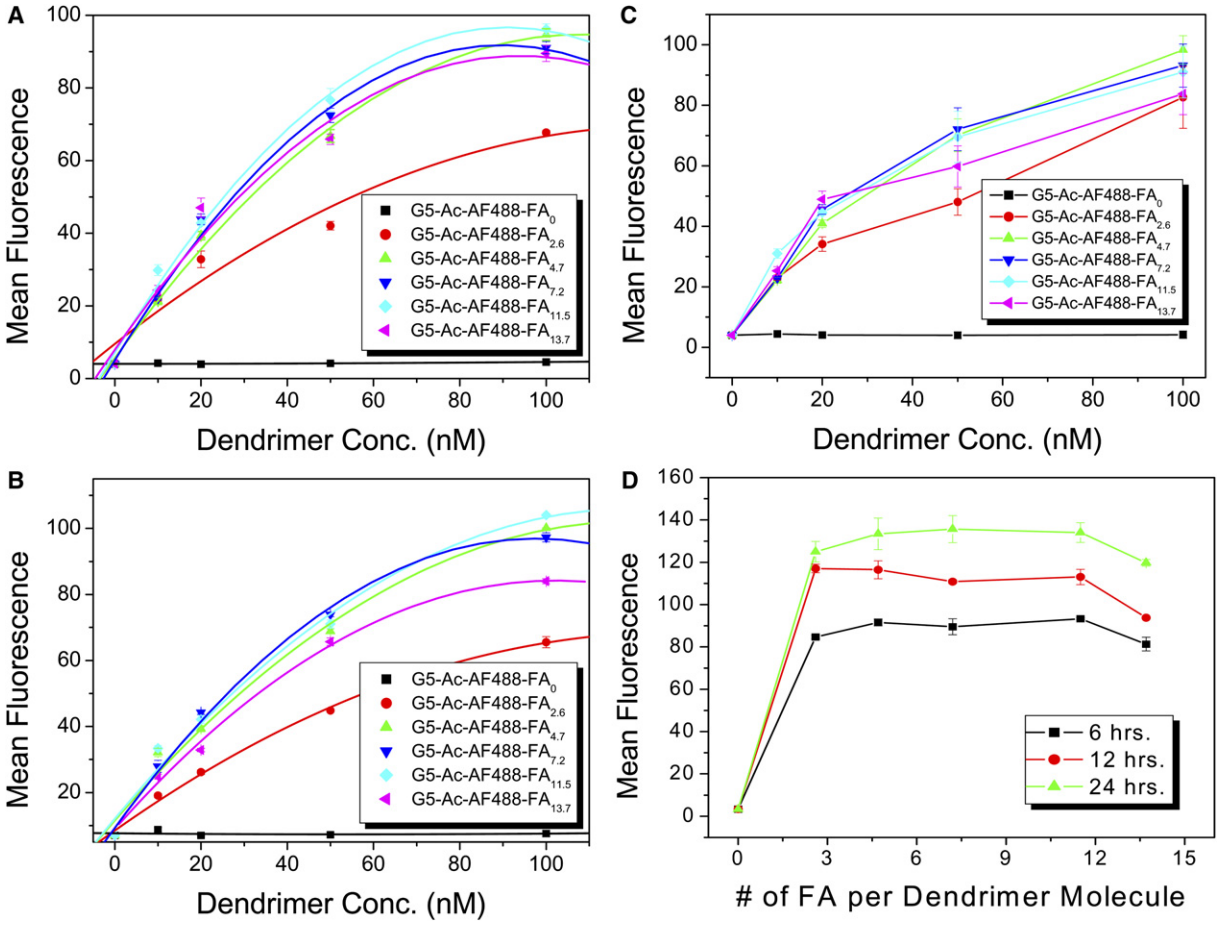

Figure 4. Binding and Uptake of Dendritic Nanodevices by FAR-Overexpressing KB Cells Measured by FACS

(A–C) Concentration-dependent binding and uptake of nanodevices (A) at 37°C for 1 hr and (B) at 4°C for 1 hr. The same experiment with (A) at the 50 and 100 nM concentrations is repeated 12 times and (C) includes all the data points from the repetitions of the experiment at 37°C for 1 hr.

(D) Time-dependent binding and uptake of dendritic nanodevices by FAR-overexpressing KB cells after 6, 12, and 24 hr incubations. The longer incubation times demonstrate that the endocytosis rates of the dendritic nanodevices are similar regardless of the FA/dendrimer ratio. The error bars represent standard deviations.

multivalency. The exponential decrease in k_d as a function of the number of folic acids per dendrimer clearly demonstrates the multivalency effects upon dissociation from surface. This analysis demonstrates that the nonlinear behavior of the equilibrium constant (K_D in Table 2 or K_A in Figure 2) arises from the effects of multivalency upon dissociation, not association, of the targeted dendrimer with the FBP.

In order to better understand the saturation behavior observed for the binding avidity, the number of FBP per unit surface area on the SPR sensor chip was calculated. The density of FBP immobilized on the chip was measured to be 8 ng/mm^2. Based upon the 30 kDa molecular weight of FBP, this translates into ~16 molecules/100 nm^2. Our previously reported experimental and theoretical work on dendrimer deformation on surfaces [34] indicates that a G5 PAMAM dendrimer molecule can deform to a disc-like structure with a radius of 4.8 nm or exhibit a maximum surface area of 72 nm^2. Based upon the measured surface density of FBP and the footprint of the deformed G5 PAMAM dendrimer, a maximum of ~12 FBP molecules can theoretically interact per G5-Ac-AF488-FA$_x$ molecule. The actual number of FBP molecules capable of an optimal binding interaction should be lower than 12 since the conformation of the FBP was not controlled. Thus, the saturation behavior observed in the SPR experiments is roughly consistent with the maximum number of properly oriented FBPs expected in an individual dendrimer's area of interaction.

The FACS experiments utilizing KB cells also showed a saturation behavior. Calculation of the number of FAR per unit area on a KB cell was carried out employing two assumptions: (1) the exposed surface of a KB cell can be computed as a spherical cap, and (2) every FAR receptor is present on the surface of the exposed apical cap. The number of FAR on a KB cell is roughly 2,400,000, according to previous measurement (T. Thomas and J.R.B., unpublished data) [35]. Given a surface area of a single KB

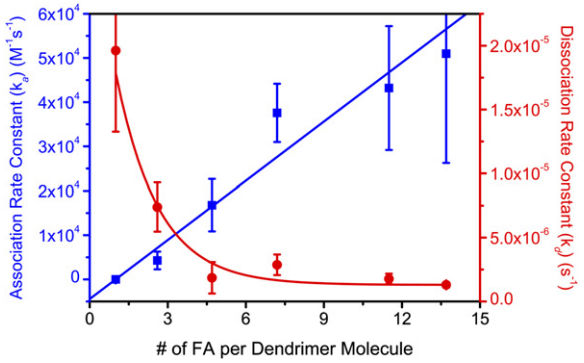

Figure 5. Association Rate Constant and Dissociation Rate Constant of Dendrimers with Varying Numbers of Folic Acid as Measured by SPR

The association rate constant (k_a) ($M^{-1}s^{-1}$) value increases linearly with the number of folic acids per dendrimer whereas the dissociation rate constant k_d (s^{-1}) value decays exponentially with the increasing number of folic acid ligands. The error bars are standard errors of the mean from $\geq$3 runs.

cell of 481.1 μm^2 ($2\pi r^2$ where r = 8.75 μm), the average FAR density is roughly 1/200 nm^2. Although the "average" computed density of FAR on a KB cell is much lower than that of FBP on the chip, recall that FAR distribution on the cell surface is known to be heterogeneous [20, 21]. Therefore, the saturation behavior observed on the cell surface is occurring within a physically reasonable range of FAR surface concentration, and is likely dependent on the FA density on the dendrimer, the total surface area reach of each dendrimer particle, and the closest packing of FAR possible on the cell surface.

The average effective spacing of FA on the dendrimer particle changes as a function of the degree of FA conjugated. Roughly speaking, it is the surface area presented by the G5 dendrimer, 72 nm^2, divided by the number of FA conjugated to the dendrimer to give 28, 15, 10, 6, and 5 nm^2, respectively, as the average effective spacing. There is no detailed structure for FAR, however it is believed to be ~30 kDa [39]. Assuming a density of 1.35 g/ml and a globular shape, this roughly corresponds to a volume of ~37 nm^3, a projection onto the dendrimer surface of ~13 nm^2, or a diameter of ~4 nm. Thus, a given G5 PAMAM dendrimer particle could not reasonably accommodate more than 72/13 or ~5–6 FAR unless the plasma membrane deformed about the dendrimer particle. Thus, the saturation of binding effect does occur about where one could reasonably expect the maximum number of FAR interactions per dendrimer particle.

It is also interesting to note the same saturation behavior is observed for data obtained at 4°C, where rapid diffusion of receptors in the membrane is not expected. The average spacing of FAR in the membrane is estimated to be ~1/200 nm^2, not the ~1/13 nm^2 suggested by the saturation behavior. This suggests that at least 5–6 folic acid receptors are aggregated in the membrane in a preorganized fashion and that the dendrimer complex does not recruit receptors via a diffusional membrane process.

We believe two related properties of the PAMAM dendrimer scaffolds likely play a key role in allowing the multiple FA/FAR interactions required to achieve efficient multivalent interactions. First, the geometry of the dendrimer preorganizes the targeting ligands into a small region of space as compared to what is obtained if one conjugates the targets to a similar molecular weight linear polymer. Thus, one has "prepaid" the entropy penalty for localizing the targeting ligands. Second, the dendrimer structure allows all targeting ligands to address the cell surface [34]. This is not necessarily the case for a similar molecular weight hyperbranched polymer in which tangled or cross-linked chains may prevent the needed ligand orientation. PAMAM dendrimers are quite flexible and easily deform from the spherical shape adopted in isotropic media to a disc-like structure upon interaction with a surface [34]. This combination of preorganization, polymer backbone topology, and easy deformability all combine to make the PAMAM dendrimer an effective material for achieving multivalent binding to cell surfaces.

SIGNIFICANCE

A quantitative and systematic study of the multivalent effect for folic acid-targeted dendritic nanodevices is presented. A dramatic enhancement of binding avidity (up to ~170,000 fold) is measured, although the rate of cellular internalization remained unchanged. Thus, the key factor in the previously reported tumor reduction is the enhanced residence time of the material on the cell, leading to greater incorporation, not binding followed by an enhanced rate of endocytosis. The multivalent effector system described herein exhibits a binding avidity improvement of 5 orders of magnitude, which represents a substantial advance over the 1–2 orders of magnitude previously reported. The study indicates that the principles of multivalency can be effectively employed to synthesize targeted chemotherapeutics with avidities great enough to give in vivo efficacy.

EXPERIMENTAL PROCEDURES

Materials

Folic acid (FA), folate binding protein extracted from bovine milk (FBP), acetic anhydride, ethylenediamine, methanol, dimethylsulfoxide (DMSO), penicillin/streptomycin, and fetal bovine serum were purchased from Sigma-Aldrich (St. Louis, MO). AlexaFluor 488 carboxylic acid linked by succinimidyl ester (AF488), Trypsin-EDTA, Dulbecco's PBS, and RPMI 1640 (with and without folic acid) were supplied by Invitrogen (Gaithersburg, MD).

Preparation of G5 PAMAM-Based Cancer Cell Targeting Nanodevices

A G5 PAMAM dendrimer was synthesized and purified to remove low molecular weight impurities as well as high molecular weight dimers according to our previous reports [29–31]. After purification, G5 PAMAM dendrimers were partially acetylated (70 of the 110 total primary amines), resulting in G5-Ac_{70} [40]. The remaining 40 primary amine groups were used for reaction to further functionalize the dendrimers. Note that a G5 PAMAM dendrimer molecule has

approximately 110 primary amine termini according to our previous titration measurement [40].

To fluorescently label the dendrimers, AF488 dissolved in DMSO was added to the dendrimer/H_2O solution at a molar ratio of 5:1 (AF488:dendrimer) in the presence of 1 M $NaHCO_3$ and the reaction mixture was stirred at RT for 48 hr. The resulting mixture of the dendrimer conjugate (G5-Ac_{70}-AF488) was then dialyzed in water for 2 days and lyophilized for 2 days, followed by 10 cycles of ultrafiltration with PBS (with Ca^{2+} and Mg^{2+}) and water using a 10,000 molecular weight cut-off membrane at 21°C, 5000 rpm for 30 min each.

G5-Ac_{70}-AF488 conjugate in H_2O was then reacted with FA preactivated by 1-[3-(dimethylamino)propyl]-3-ethylcarbodiimide/HCl (EDC) in DMF/DMSO at different molar ratios (3:1, 6:1, 9:1, 12:1, 15:1) of FA to G5-Ac_{70}-AF488. The same purification process was carried out as described in the AF488 conjugation. Lastly, full acetylation of the remaining primary amine group was completed [40], yielding our final products G5-Ac-AF488-FA_0, G5-Ac-AF488-$FA_{2.6}$, G5-Ac-AF488-$FA_{4.7}$, G5-Ac-AF488-$FA_{7.2}$, G5-Ac-AF488-$FA_{11.5}$, and G5-Ac-AF488-$FA_{13.7}$. Note that the numbers in subscript following FA in the dendrimer nomenclature are determined by GPC results in Table 1.

Characterization of G5 PAMAM-Based Cancer Cell Targeting Nanodevices

^{1}H NMR spectra were taken in D_2O and were used to provide integration values for structural analysis using a Bruker AVANCE DRX 500 instrument following the same method described earlier [40, 41]. UV/Vis spectra of the dendrimer conjugates were measured on a Perkin Elmer UV/Vis spectrometer Lambda 20 (Wellesley, MA). The standard curve for concentration was determined using free, molecular FA. This causes the dendrimer-FA conjugates to appear artificially low due to the expected deviation in Beer's Law for these spatially constrained samples. HPLC and GPC measurements were performed according to the general methods previously reported [32, 33]. GPC experiments were performed using an Alliance Waters 2695 separations module (Waters Corp., Milford, MA) equipped with a Waters 2487 dual-channel UV detector (Waters Corp.), a Wyatt Dawn DSP laser photometer (Wyatt Technology Corp., Santa Barbara, CA), an Optilab DSP interferometric refractometer (Wyatt Technology Corp.), and TosoHaas TSK-Gel (Tosoh Bioscience LLC, Montgomeryville, PA) Guard PHW (75 × 7.5 mm, 12 μm), G 2000 PW (300 × 7.5 mm, 10 μm), G 3000 PW (300 × 7.5 mm, 10 μm), and G 4000 PW (300 × 7.5 mm, 17 μm) columns. Column temperatures were maintained at 25 ± 0.2°C with a Waters temperature control module. Citric acid buffer (0.1 M) with 0.025% sodium azide in water was used as a mobile phase. The pH of the mobile phase was adjusted to 2.74 using NaOH, and the flow rate was maintained at 1 ml/min. Sample concentration was approximately 2 mg/ml, and an injection volume of 100 μl was used for all samples. Molar mass moments of the polymers were determined using Astra software (version 4.9) (Wyatt Technology Corp.). Polyethylene glycol (PEG) with molecular weight of 15 kDa (Sigma-Aldrich, St. Louis, MO) was used as a standard to confirm the accuracy of the results. Alternatively, G5 PAMAM dendrimer prepared at MNiMBS was also used to crosscheck the obtained molecular weight data. Additional details regarding the HPLC experiments are provided with the chromatograms in the supplementary information.

Surface Plasmon Resonance Measurements

To study the interaction of FA-conjugated G5 PAMAM-based nanodevices (G5-Ac-AF488-FA_x: x = 2.6, 4.7, 7.2, 11.5, or 13.7) with the FBP, the surface plasmon resonance (SPR) technique using BIAcore X (Pharmacia Biosensor AB, Uppsala, Sweden) was employed. FBP was immobilized on the sensor chip surface (channel 2) of a carboxylated dextran-coated gold film (CM 5 sensor chip) by amine coupling as described elsewhere [3–5, 42]. Briefly, 70 μl of a mixed solution of NHS/ECD (1:1, v/v) was first injected into the BIAcore to activate the carboxylated dextran, followed by injection of 70 μl of 2.5 mg/ml FBP dissolved in 100 mM potassium phosphate buffer (pH 5.0), supplemented with 4 mM mercaptoethanol and 10% (v/v) glycerol. 1 M ethanolamine in water (pH 8.5) was then injected to deactivate residual NHS-esters on the sensor chip. The immobilization process was performed at a flow rate of 10 μl/min, resulting in the binding of ~8 ng/mm^2 (~8000 RU) of FBP per channel. The dendritic nanodevices (30 μl) were injected at concentrations of 500 nM, 1 μM, and 2 μM at a flow rate of 10 μl/min, allowing the nanodevices to flow in both channels (channel 1 for reference and channel 2 with FBP) for 3 min. The final SPR sensorgrams were obtained from the signals from channel 2 subtracted by those from channel 1. Binding parameters of free FA with FBP were evaluated by the same condition but at different concentrations (1 and 2 mM used for free FA). After each measurement, 5 μl of 10 mM glycidol-HCl at pH 1.5 was injected to regenerate the surface of the chip. It should be noted that we use term affinity for monovalent systems and avidity for multivalent systems in this paper.

The binding curves were fit using the 1:1 Langmuir binding model in BIAevaluation software. Associations and dissociations were fit separately since there was turbulence in the curves between association and dissociation phases in the process of subtracting signals from the reference channel. Dissociation constants (K_D) for each dendrimer were obtained by averaging at least three different sets of results which had χ^2 values lower than 3.0. All runs were independently analyzed for errors associated with mass transport by exporting the data files to Excel and plotting dR/dt versus R following the analysis described by Glaser [43]. All of the resulting plots showed excellent linearity and no evidence of the negative curvature associated with mass transport. For all experiments, the analyte concentrations were greater than the measured K_D values by 3–4 orders of magnitude, verifying that the first derivative plots were a meaningful method for ruling out mass transport effects.

Cell Culture and Flow Cytometry (Fluorescence Activated Cell Sorter: FACS) Measurements

The KB cell line was purchased from the American Type Tissue Collection (ATCC, Manassas, VA) and grown continuously as a monolayer at 37°C and 5% CO_2 in RPMI 1640 medium (Mediatech, Herndon, VA). The RPMI 1640 medium was supplemented with penicillin (100 units/ml), streptomycin (100 μg/ml), and 10% heat-inactivated fetal bovine calf serum (FBS) before use. KB cells were cultured in RPMI 1640 medium without folic acid (Mediatech) for at least 4 days before experiments, resulting in the folic acid receptor overexpressing KB (FAR-KB) cell line.

For the FACS measurements, the FAR-KB cells were seeded on a 24-well plate for tissue culture at a concentration of 2 × 10^5 cells/well and grown in folic acid deficient RPMI 1640 media (Mediatech, Herndon, VA) at 37°C, 5% CO_2 for 24 hr. The cells were then incubated with the series of the prepared nanodevices at either 37°C or 4°C for 1 hr. After removal of supernatants, cells were trypsinized and collected into FACS tubes, followed by centrifugation at 1500 rpm for 5 min to obtain cell pellets. The pellets were washed with PBS (Ca^{2+}, Mg^{2+}) twice using a repetitive centrifugation and resuspension process and then finally resuspended in PBS with 0.1% bovine serum albumin. The FACS sample preparation was performed on ice to inhibit cellular reactions such as further uptake. Fluorescence signal intensities from the samples were measured using a Coulter EPICS/XL MCL Beckman-Coulter flow cytometer, and data were analyzed using Expo32 software (Beckman-Coulter, Miami, FL) [32].

Confocal Laser Scanning Microscopy (CLSM) Observation

FAR-KB cells were plated on a glass bottomed Petri dish. The cell culture medium was replaced by 2 ml of each dendrimer nanodevice solution in PBS (Ca^{2+}, Mg^{2+}), followed by incubation at 37°C under 5% CO_2 for 1 hr. The nanodevice-containing solution was removed, and the resulting cell monolayer was washed with PBS at least three times. Cells were fixed with 2% formaldehyde in PBS at room temperature for 10 min and then washed twice with PBS. Cells were stained by DAPI and conserved in an antiphotobleaching agent. Confocal images were then taken on an Olympus FV-500 confocal microscope using a 100×, 1.4 NA oil immersion objective. To visualize AF_{488} attached

on dendrimers, the 488 nm line of an argon ion laser was used for excitation, and the emission was filtered at 505–525 IF nm.

Supplemental Data

The Supplemental Data include figures showing ^{1}H NMR, UV/Vis, HPLC, and GPC results (Figures S1–S4) of the prepared dendrimer nanodevices. Figures S5 and S6 show FACS and fluorescence microscopy data, respectively, indicating that the targeted nanodevices specifically interact with target cells (FAR-overexpressing KB cells). The SPR traces are shown in Figure S7. The Supplemental Data are available at http://www.chembiol.com/cgi/content/full/14/1/107/DC1/.

ACKNOWLEDGMENTS

This work has been funded with federal funds from the National Cancer Institute, National Institutes of Health, under contract # N01-CO-27173. This research has been also supported by State of Michigan MEDC funding under GR-472, grant # 085P3000548. The University of Michigan has licensed this technology to a start-up company, Avidimer Therapeutics, and Dr. Baker has a significant equity position in this entity. The authors thank Ankur Desai for his assistance with GPC measurements.

Received: June 5, 2006
Revised: September 14, 2006
Accepted: November 1, 2006
Published: January 26, 2007

REFERENCES

1. Hilgenbrink, A.R., and Low, P.S. (2005). Folate receptor-mediated drug targeting: from therapeutics to diagnostics. J. Pharm. Sci. *94*, 2135–2146.
2. Lu, Y.J., and Low, P.S. (2002). Folate-mediated delivery of macromolecular anticancer therapeutic agents. Adv. Drug Deliv. Rev. *54*, 675–693.
3. Salmaso, S., Semenzato, A., Caliceti, P., Hoebeke, J., Sonvico, F., Dubernet, C., and Couvreur, P. (2004). Specific antitumor targetable beta-cyclodextrin-poly(ethylene glycol)-folic acid drug delivery bioconjugate. Bioconjug. Chem. *15*, 997–1004.
4. Sonvico, F., Mornet, S., Vasseur, S., Dubernet, C., Jaillard, D., Degrouard, J., Hoebeke, J., Duguet, E., Colombo, P., and Couvreur, P. (2005). Folate-conjugated iron oxide nanoparticles for solid tumor targeting as potential specific magnetic hyperthermia mediators: synthesis, physicochemical characterization, and in vitro experiments. Bioconjug. Chem. *16*, 1181–1188.
5. Stella, B., Arpicco, S., Peracchia, M.T., Desmaele, D., Hoebeke, J., Renoir, M., D'Angelo, J., Cattel, L., and Couvreur, P. (2000). Design of folic acid-conjugated nanoparticles for drug targeting. J. Pharm. Sci. *89*, 1452–1464.
6. Quintana, A., Raczka, E., Piehler, L., Lee, I., Myc, A., Majoros, I., Patri, A.K., Thomas, T., Mule, J., and Baker, J.R. (2002). Design and function of a dendrimer-based therapeutic nanodevice targeted to tumor cells through the folate receptor. Pharm. Res. *19*, 1310–1316.
7. Kiessling, L.L., Gestwicki, J.E., and Strong, L.E. (2006). Synthetic multivalent ligands as probes of signal transduction. Angew. Chem. Int. Ed. Engl. *45*, 2348–2368.
8. Lee, R.T., and Lee, Y.C. (2000). Affinity enhancement by multivalent lectin-carbohydrate interaction. Glycoconj. J. *17*, 543–551.
9. Lee, Y.C., and Lee, R.T. (1995). Carbohydrate-protein interactions—basis of glycobiology. Acc. Chem. Res. *28*, 321–327.
10. Mammen, M., Choi, S.K., and Whitesides, G.M. (1998). Polyvalent interactions in biological systems: implications for design and use of multivalent ligands and inhibitors. Angew. Chem. Int. Ed. Engl. *37*, 2755–2794.
11. Metallo, S.J., Kane, R.S., Holmlin, R.E., and Whitesides, G.M. (2003). Using bifunctional polymers presenting vancomycin and fluorescein groups to direct anti-fluorescein antibodies to self-assembled monolayers presenting D-alanine-D-alanine groups. J. Am. Chem. Soc. *125*, 4534–4540.
12. Mourez, M., Kane, R.S., Mogridge, J., Metallo, S., Deschatelets, P., Sellman, B.R., Whitesides, G.M., and Collier, R.J. (2001). Designing a polyvalent inhibitor of anthrax toxin. Nat. Biotechnol. *19*, 958–961.
13. Seeberger, P.H., and Werz, D.B. (2005). Automated synthesis of oligosaccharides as a basis for drug discovery. Nat. Rev. Drug Discov. *4*, 751–763.
14. Christensen, T., Gooden, D.M., Kung, J.E., and Toone, E.J. (2003). Additivity and the physical basis of multivalency effects: a thermodynamic investigation of the calcium EDTA interaction. J. Am. Chem. Soc. *125*, 7357–7366.
15. Reuter, J.D., Myc, A., Hayes, M.M., Gan, Z.H., Roy, R., Qin, D.J., Yin, R., Piehler, L.T., Esfand, R., Tomalia, D.A., et al. (1999). Inhibition of viral adhesion and infection by sialic-acid-conjugated dendritic polymers. Bioconjug. Chem. *10*, 271–278.
16. Kitov, P.I., and Bundle, D.R. (2003). On the nature of the multivalency effect: a thermodynamic model. J. Am. Chem. Soc. *125*, 16271–16284.
17. Gestwicki, J.E., Cairo, C.W., Mann, D.A., Owen, R.M., and Kiessling, L.L. (2002). Selective immobilization of multivalent ligands for surface plasmon resonance and fluorescence microscopy. Anal. Biochem. *305*, 149–155.
18. Rao, J.H., Lahiri, J., Isaacs, L., Weis, R.M., and Whitesides, G.M. (1998). A trivalent system from vancomycin center dot D-Ala-D-Ala with higher affinity than avidin·biotin. Science *280*, 708–711.
19. Ross, J.F., Chaudhuri, P.K., and Ratnam, M. (1994). Differential regulation of folate receptor isoforms in normal and malignant-tissues in-vivo and in established cell-lines—physiological and clinical implications. Cancer *73*, 2432–2443.
20. Weitman, S.D., Weinberg, A.G., Coney, L.R., Zurawski, V.R., Jennings, D.S., and Kamen, B.A. (1992). Cellular-localization of the folate receptor—potential role in drug toxicity and folate homeostasis. Cancer Res. *52*, 6708–6711.
21. Weitman, S.D., Lark, R.H., Coney, L.R., Fort, D.W., Frasca, V., Zurawski, V.R., and Kamen, B.A. (1992). Distribution of the folate receptor gp38 in normal and malignant-cell lines and tissues. Cancer Res. *52*, 3396–3401.
22. Campbell, I.G., Jones, T.A., Foulkes, W.D., and Trowsdale, J. (1991). Folate-binding protein is a marker for ovarian-cancer. Cancer Res. *51*, 5329–5338.
23. Leamon, C.P., and Low, P.S. (1994). Selective targeting of malignant-cells with cytotoxin-folate conjugates. J. Drug Target. *2*, 101–112.
24. Leamon, C.P., and Reddy, J.A. (2004). Folate-targeted chemotherapy. Adv. Drug Deliv. Rev. *56*, 1127–1141.
25. Roy, E.J., Gawlick, U., Orr, B.A., and Kranz, D.M. (2004). Folate-mediated targeting of T cells to tumors. Adv. Drug Deliv. Rev. *56*, 1219–1231.
26. Stephenson, S.M., Low, P.S., and Lee, R.J. (2004). Folate receptor-mediated targeting of liposomal drugs to cancer cells. Methods Enzymol. *387*, 33–50.
27. Kranz, D.M., Patrick, T.A., Brigle, K.E., Spinella, M.J., and Roy, E.J. (1995). Conjugates of folate and anti-T-cell-receptor antibodies specifically target folate-receptor-positive tumor-cells for lysis. Proc. Natl. Acad. Sci. USA *92*, 9057–9061.
28. Patri, A.K., Majoros, I.J., and Baker, J.R. (2002). Dendritic polymer macromolecular carriers for drug delivery. Curr. Opin. Chem. Biol. *6*, 466–471.

29. Kukowska-Latallo, J.F., Candido, K.A., Cao, Z.Y., Nigavekar, S.S., Majoros, I.J., Thomas, T.P., Balogh, L.P., Khan, M.K., and Baker, J.R. (2005). Nanoparticle targeting of anticancer drug improves therapeutic response in animal model of human epithelial cancer. Cancer Res. *65*, 5317–5324.
30. Majoros, I.J., Thomas, T.P., Mehta, C.B., and Baker, J.R. (2005). Poly(amidoamine) dendrimer-based multifunctional engineered nanodevice for cancer therapy. J. Med. Chem. *48*, 5892–5899.
31. Hong, S., Bielinska, A.U., Mecke, A., Keszler, B., Beals, J.L., Shi, X.Y., Balogh, L., Orr, B.G., Baker, J.R., and Banaszak Holl, M.M. (2004). Interaction of poly(amidoamine) dendrimers with supported lipid bilayers and cells: hole formation and the relation to transport. Bioconjug. Chem. *15*, 774–782.
32. Hong, S., Leroueil, P.R., Janus, E.K., Peters, J.L., Kober, M.-M., Islam, M.T., Orr, B.G., Baker, J.R., and Banaszak Holl, M.M. (2006). The interaction of polycationic polymers with supported lipid bilayers and cells: nanoscale hole formation and enhanced membrane permeability. Bioconjug. Chem. *17*, 728–734.
33. Islam, M.T., Majoros, I.J., and Baker, J.R. (2005). HPLC analysis of PAMAM dendrimer based multifunctional devices. J. Chromatogr. B Analyt. Technol. Biomed. Life Sci. *822*, 21–26.
34. Mecke, A., Lee, I., Baker, J.R., Holl, M.M.B., and Orr, B.G. (2004). Deformability of poly(amidoamine) dendrimers. Eur. Phys. J. E *14*, 7–16.
35. Kane, M.A., Elwood, P.C., Portillo, R.M., Antony, A.C., Najfeld, V., Finley, A., Waxman, S., and Kolhouse, J.F. (1988). Influence on immunoreactive folate-binding proteins of extracellular folate concentration in cultured human-cells. J. Clin. Invest. *81*, 1398–1406.
36. Shaunak, S., Thomas, S., Gianasi, E., Godwin, A., Jones, E., Teo, I., Mireskandari, K., Luthert, P., Duncan, R., Patterson, S., et al. (2004). Polyvalent dendrimer glucosamine conjugates prevent scar tissue formation. Nat. Biotechnol. *22*, 977–984.
37. Thomas, T.P., Majoros, I.J., Kotlyar, A., Kukowska-Latallo, J.F., Bielinska, A., Myc, A., and Baker, J.R. (2005). Targeting and inhibition of cell growth by an engineered dendritic nanodevice. J. Med. Chem. *48*, 3729–3735.
38. Thomas, T.P., Patri, A.K., Myc, A., Myaing, M.T., Ye, J.Y., Norris, T.B., and Baker, J.R. (2004). In vitro targeting of synthesized antibody-conjugated dendrimer nanoparticles. Biomacromolecules *5*, 2269–2274.
39. Holm, J., Hansen, S.I., Hoier-Madsen, M., Birn, H., and Helkjaer, P.E. (1999). High-affinity folate receptor in human ovary, serous ovarian adenocarcinoma, and ascites: radioligand binding mechanism, molecular size, ionic properties, hydrophobic domain, and immunoreactivity. Arch. Biochem. Biophys. *366*, 183–191.
40. Majoros, I.J., Keszler, B., Woehler, S., Bull, T., and Baker, J.R. (2003). Acetylation of poly(amidoamine) dendrimers. Macromolecules *36*, 5526–5529.
41. Choi, Y., Thomas, T., Kotlyar, A., Islam, M.T., and Baker, J.R. (2005). Synthesis and functional evaluation of DNA-assembled polyamidoamine dendrimer clusters for cancer cell-specific targeting. Chem. Biol. *12*, 35–43.
42. Nygren-Babol, L., Sternesjo, A., Jagerstad, M., and Bjorck, L. (2005). Affinity and rate constants for interactions of bovine folate-binding protein and folate derivatives determined by optical biosensor technology. Effect of stereoselectivity. J. Agric. Food Chem. *53*, 5473–5478.
43. Glaser, R.W. (1993). Antigen-antibody binding and mass-transport by convection and diffusion to a surface—a 2-dimensional computer-model of binding and disscociation kinetics. Anal. Biochem. *213*, 152–161.

